Journal of Advanced Marine Engineering and Technology, Vol. 45, No. 6, pp. 371~379, 2021
J. Advanced Marine Engineering and Technology (JAMET)
https://doi.org/10.5916/jamet.2021.45.6.371

ISSN 2234-7925 (Print)
ISSN 2765-4796 (Online)
Original Paper

Performance of single-channel pump based on various impeller flow passage shape design parameters

Thi Hong Minh Hoang[1] · Ujjwal Shrestha[2] · Young-Do Choi†

(Received August 31, 2021 ; Revised October 6, 2021 ; Accepted December 13, 2021)

Abstract: A single-channel pump is widely used as a non-clog sewage pump for drainage and wastewater control systems. It comprises a free-passage impeller and is suitable for managing solids without clogging; as such, it allows the transfer of live fishes, eels, and shrimps. The design method of a single-channel pump differs from that of a general pump. In this study, various pump design parameters are evaluated. Numerical analysis is conducted to investigate the single-channel pump performance. Based on a parametric study, a suitable design for a single-channel pump is developed. Furthermore, three impeller cross-sections are investigated to improve the efficiency and suction performance of the pump.

Keywords: Single channel pump, Pump performance, Impeller flow passage, Design parameter

1. Introduction

The single-channel pump is used in industry, agriculture, and aquaculture. In addition to the transfer of wastewater and sewage solids in the industry, the transfer of live fishes, eels, shrimps, fruits, and vegetables is essential in the aquaculture and agriculture fields. Compared with a centrifugal pump, a single-channel pump comprises a unique impeller **[1]**. The single-channel pump impeller has a free passage from the impeller suction for discharge; furthermore, it affords a large capacity and solid handling capability. Therefore, it allows the transfer of fruits, vegetables, and live fishes without causing clogging or damage.

Owing to the unique and specific structure of the single-channel pump impeller, studies pertaining to single-channel pumps have been conducted extensively. Kim *et al.* **[2]** designed and optimized a single-channel pump for wastewater treatment and vibration reduction during an impeller–volute interaction. Guo *et al.* **[3]** investigated the effect of impeller blade thickness on the pump performance and internal flow characteristics of a single-channel pump model. Wu *et al.* **[4]** predicted the performance of a single-channel pump using various turbulence models. Keays *et al.* **[5]** investigated the behavior of a single-blade wastewater pump using numerical and experimental methods. The numerical results indicated that the complicated flow behind the trailing edge contributed primarily to power loss and low efficiency. Pei *et al.* **[6]** suggested a fluid structural interaction analysis to quantitatively obtain the coupling effects of a fluid-structure system in a single-blade centrifugal pump on unsteady flows; furthermore, they reduced the pressure fluctuation and increased the reliability of the pump. Litfin *et al.* **[7]** conducted a numerical and experimental investigation of the trailing-edge modifications of centrifugal pump wastewater pump impellers.

The aim of this study was to conceptually design a single-channel pump to prepare a detailed design and model test. A parametric study of impeller shape design was conducted to improve pump performance.

2. Design of Single Channel Pump

The design specifications of the single-channel pump model are listed in **Table 1**. The specific speed of the single-channel pump is calculated as follows:

$$N_s = \frac{3.65n\sqrt{Q}}{H^{0.75}} \quad (1)$$

Figure 1 presents three-dimensional and two-dimensional views of the single-channel pump impeller casing. The design parameters of the single-channel pump were calculated based on

† Corresponding Author (ORCID: http://orcid.org/0000-0001-7316-1153): Professor, Department of Mechanical Engineering, Institute of New and Renewable Energy Technology Research, Mokpo National University, 1666 Youngsan-ro, Cheonggye-myeon, Muan-gun, Jeonnam, 58554, Korea, E-mail: ydchoi@mnu.ac.kr, Tel: 061-450-2419

1 M. S. Candidate, Graduate School, Department of Mechanical Engineering, Mokpo National University, E-mail: hoanghongminh13@gmail.com

2 Ph. D. Candidate, Graduate School, Department of Mechanical Engineering, Mokpo National University, E-mail: d19541301@365.mokpo.ac.kr

Table 1: Design specifications of single-channel pump

Item	Nomenclature	Units	Value
Flow rate	Q	m^3/s	0.064
Total head	H	m	4
Rotational speed	n	min^{-1}	650
Specific speed	N_s	[min^{-1}, m, m^3/s]	212

Table 2: Design parameters for initial model of single-channel pump impeller

Item	Nomenclature [Unit]	Range **[1]**	Initial value
Impeller outlet diameter	D_2 $[mm]$		330
Coefficient of impeller outlet diameter	K_{D_2}	9.8-10.3	10.3
Impeller inlet diameter	D_1 $[mm]$		185
Coefficient of impeller inlet diameter	K_{D_1}	3.8-4.5	4
Outlet angle of line 1	β_0 [°]		37
Total wrap angle of line 1	φ_1 [°]		150
Inlet angle of line 3	β_1 [°]		8
Outlet angle of line 3	β_2 [°]		10
Total wrap angle of line 3	φ_2 [°]		297

a previous study **[1]**, as shown in **Table 2**. The single-channel pump impeller was designed by establishing inlet and outlet components. The inlet and outlet of the impeller were formed by sweeping the cross sections following the centerline (Line 1) and Line 3, respectively. Line 1 can be modified by changing β_0. Line 3 can be modified by changing D_1, D_2, β_1, or β_2. The detailed design method of the single-channel pump impeller is presented in previous publications **[1][3]**. The various impeller shapes determined based on D_1, D_2, β_0, β_1, and β_2 can significantly affect the hydraulic pump performance. Therefore, the effects of the abovementioned design parameters on the pump performance of a single-channel pump impeller must be investigated. The equation for Line 1 is as follows:

$$\begin{cases} r_{1i} = 0.00721\varphi_{1i}^2 \\ z = 250\left[1-\left(1-\dfrac{\varphi_{1i}}{151}\right)\right] \\ \varphi_{1i} = 151t\ (0<t<1) \end{cases} \tag{2}$$

Line 2 is at the edge of the inlet, which is observed when the impeller is cut by plane A–A. The equation for Line 3 is as follows:

$$\begin{cases} r_{2i} = 72.5\left[\dfrac{cos37}{cos\left(\frac{2}{297}\varphi_{2i}+8\right)}\right]^{148.5} \\ \varphi_{2i} = 297t\ (0<t<1) \\ z = 250 \end{cases} \tag{3}$$

where r_1 and r_2 are the polar radii of Lines 1 and 3, respectively; φ_1 and φ_2 are the total wrap angles of Lines 1 and 3, respectively; z is the axial length; i is the number of points; t is the non-dimensional time interval.

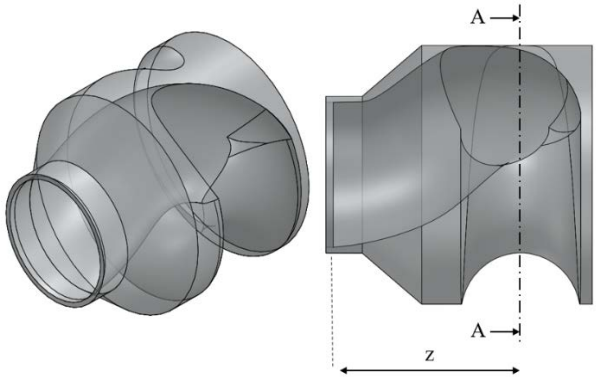

(a) Three-dimensional impeller casing

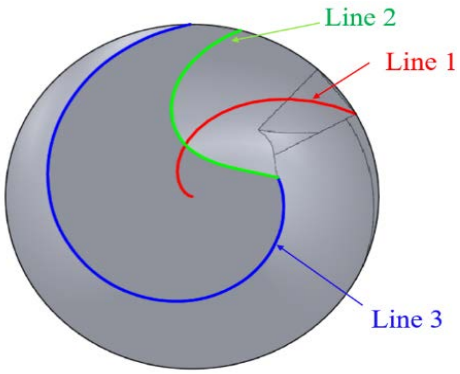

(b) Three-dimensional impeller casing at A–A view

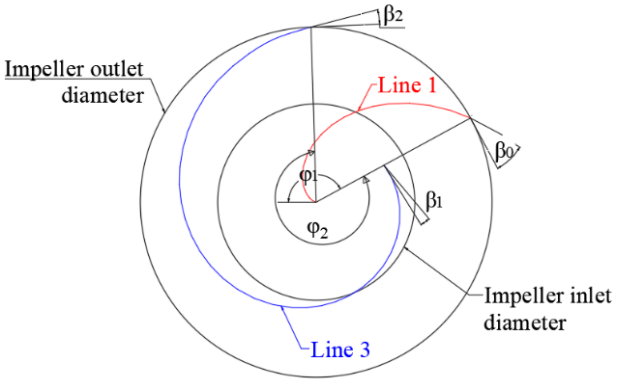

(c) Definition of geometry relationship

Figure 1: Schematic view of single-channel pump impeller

In this study, the volute casing of a single-channel pump was designed via the typical design process of a centrifugal pump casing with a circular cross-section **[8]**. **Figure 2** shows the design process for a single-channel pump volute casing. As shown in **Figure 2(a)**, the width b of the cross-sectional volute is

connected to the outlet of the impeller, and the design variable R is controlled for the cross-sectional areas based on the Stepanoff theory. The cross-sectional area distribution of the volute casing is proportional to θ, as shown in **Figure 2(c)**.

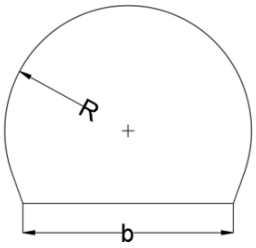

(a) Circular cross-sectional area of volute

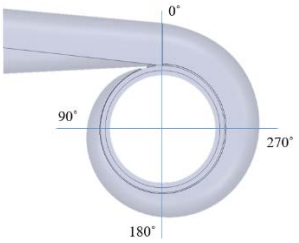

(b) Volute geometry

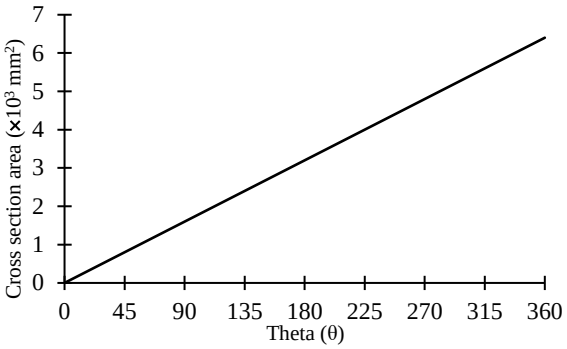

(c) Cross-sectional area distribution of volute

Figure 2: Single-channel pump volute design

3. Numerical Method

A CFD analysis was performed to evaluate the pump performance and internal flow characteristics of a single-channel pump. The commercial code ANSYS CFX 18.1 **[9]** was employed for all numerical simulations. A hexahedral mesh was generated using ANSYS ICEM 18.1 **[10]**. The numerical grids of the impeller and volute casing fluid domains for the initial model are shown in **Figure 3**. Moreover, a mesh dependence test for the initial model was performed, as shown in **Figure 4**. The mesh dependence test showed a stable pump efficiency (η) and y^+ values based on calculations using **Equations (4)** and **(5),** respectively. The CFD analysis for the single-channel pump model was conducted using 2.7 million nodes.

$$\eta = \frac{\rho g H Q}{\tau \omega} \tag{4}$$

$$y+= \frac{y U_T}{\upsilon}, \tag{5}$$

where ρ, g, H, Q, τ, and ω are the density of water, acceleration due to gravity, head, flow rate, torque, and angular velocity, respectively; y, U_T, and υ are the absolute distance from the wall, friction velocity, and kinematic viscosity, respectively.

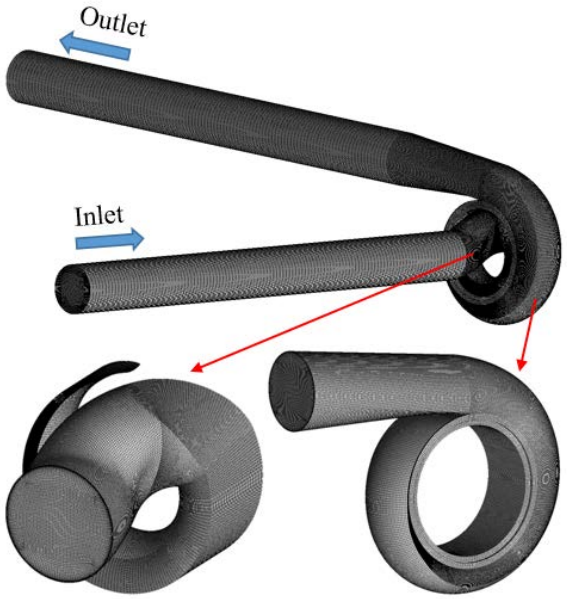

Figure 3: Numerical grids for single-channel pump impeller and volute

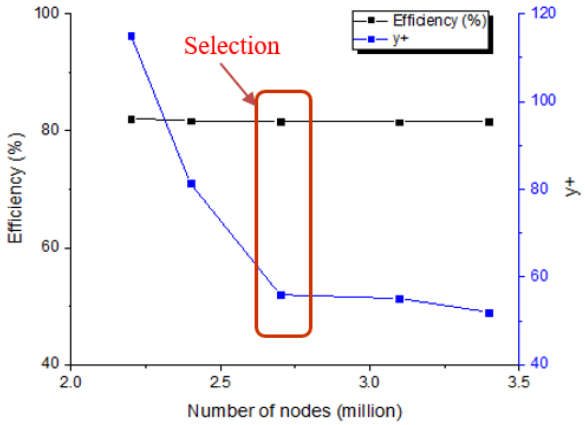

Figure 4: Results of mesh dependence test

Table 3: Numerical method and boundary condition

Analysis type	Steady state
Turbulence model	Shear stress transport
Cavitation model	Rayleigh–Plesset
Working fluid	Water at 25 °C
	Water vapor at 25 °C
Inlet	Total pressure [Pa]
Outlet	Mass flow rate [m^3/s]
Rotor–stator interface	Frozen rotor
Walls	No slip wall

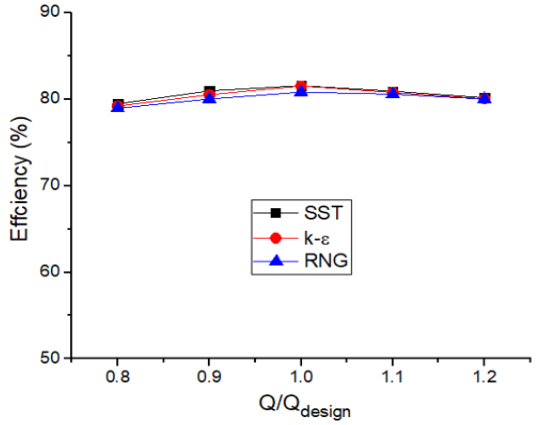

Figure 5: Results of turbulence model dependence test

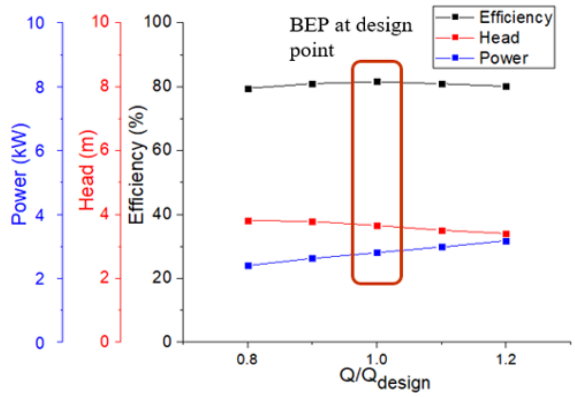

Figure 6: Pump performance curves for initial model of single-channel pump

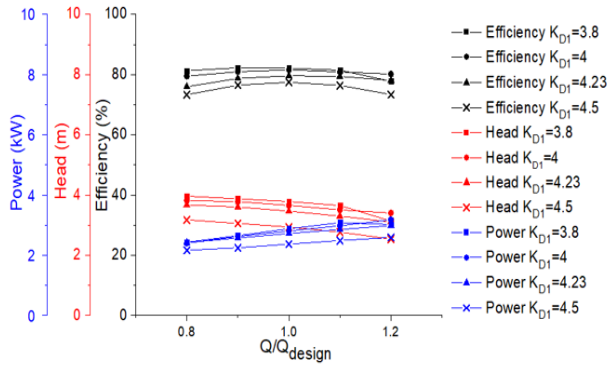

Figure 7: Effect of impeller inlet diameter on pump performance

Table 4: Impeller design parameters with different impeller inlet diameter coefficients

Inlet diameter coefficient (K_{D_1})	**3.8**	**4**	**4.23**	**4.5**
Outlet diameter coefficient (K_{D_2})	10.3	10.3	10.3	10.3
Angle (β_1)	8	8	8	8
Angle (β_2)	10	10	10	10
Angle (β_0)	37	37	37	37

Steady-state analysis was prioritized in this study. Therefore, κ–ε, RNG κ–ε, and shear stress transport (*SST*) turbulence models were employed to conduct the turbulence model dependence test, as shown in **Figure 5**. All the turbulence models adopted exhibited pump efficiency. The *SST* turbulence model is typically used for estimating separation and swirling flows on a wall. Therefore, the *SST* turbulence model was used to model the complicated flow field of fluid machinery in this study **[11]**.

The numerical method and boundary conditions used for the steady-state analysis in this study are listed in **Table 3**. The Rayleigh–Plesset model was adopted to evaluate the cavitation in the single-channel pump. The working fluids were water and water vapor at 25 °C, with a saturated vapor pressure p_v of 3170 Pa. The flow rate at the outlet was varied from 0.8 to 1.2 for analysis.

4. Results and Discussion

4.1 Performance curves based on pump initial model

Based on the design parameters of the initial impeller model for the single-channel pump listed in **Table 2**, **Figure 6** shows the performance curve of the initial single-channel pump. The best efficient point (BEP) was consistent with the design point (Q/Q_{design} = 1.0), which implies that the selected design method is accurate. The effects of impeller design parameters on hydraulic pump performance must be investigated.

4.2 Effects of impeller design parameters on pump performance

The impeller design parameters affect the impeller flow passage shape and pump performance. Therefore, the impeller design parameters were evaluated to identify their effects on pump performance. The design parameter range was obtained from a previous paper **[1]** and is shown in **Table 2**.

4.2.1 Effect of impeller inlet diameter

The coefficient of the impeller inlet diameter, K_{D_1}, was used to calculate the inlet diameter of the impeller. **Table 4** lists the impeller design parameters for the different impeller inlet diameter coefficients. **Figure 7** shows the performance curves of the single-channel pump for various K_{D_1} values. The pump performance curves indicate that the pump efficiency and head decreased as the inlet diameter increased. However, because a smaller inlet diameter resulted in a smaller single-channel pump impeller flow passage, the BEP appeared at a low flow rate region.

4.2.2 Effect of impeller outlet diameter

The coefficient of the impeller outlet diameter, K_{D_2}, was used to calculate the outlet diameter of the impeller. **Table 5** lists the impeller design parameters for the different impeller outlet diameter coefficients. **Figure 8** shows the performance curves of the single-channel pump for various K_{D_2}.

Table 5: Impeller design parameters with different impeller outlet diameter coefficients

Inlet diameter coefficient (K_{D_1})	4	4	4
Outlet diameter coefficient (K_{D_2})	**9.8**	**10.1**	**10.3**
Angle (β_1)	8	8	8
Angle (β_2)	10	10	10
Angle (β_0)	37	37	37

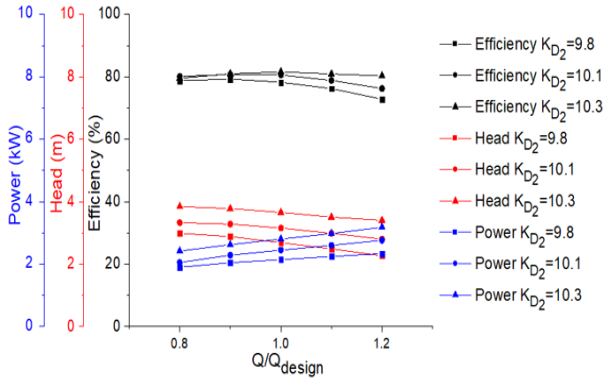

Figure 8: Effect of impeller outlet diameter on pump performance

The result is similar to the effect of the impeller inlet diameter on pump performance. When the impeller outlet diameter decreased, the best efficiency point shifted to the partial flow rate region. The single-channel pump impeller outlet diameter significantly affected the pump performance curves. When the impeller outlet diameter increased, the pump efficiency and head increased. K_{D_2}= 10.3 afforded the highest efficiency at the design point.

4.2.3. Effect of inlet angle of Line 3

Table 6 lists the impeller parameters for different inlet angles of Line 3. **Figure 9** shows the performance curves of the single-channel pump for various β_1 values. When the impeller inlet angle β_1 increased, the pump head increased slightly. β_1= 9° was selected as a base model parameter because the pump efficiency based on β_1= 9° was better than that based on other β_1 values, and the BEP was consistent with the design point. However, the BEP values of β_1= 11° and β_1= 12° did not correspond to the design point. Hence, the change in the inlet angle of Line 3 did not significantly affect the change in the performance curves.

Table 6: Impeller design parameters with different inlet angles of Line 3, $\boldsymbol{\beta_1}$

Inlet diameter coefficient (K_{D_1})	4	4	4	4
Outlet diameter coefficient (K_{D_2})	10.3	10.3	10.3	10.3
Angle (β_1)	**8**	**9**	**11**	**12**
Angle (β_2)	10	10	10	10
Angle (β_0)	37	37	37	37

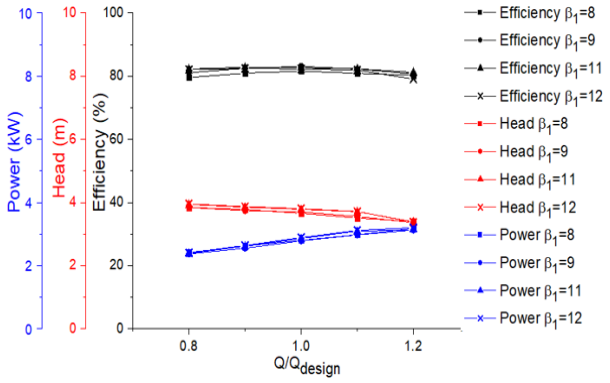

Figure 9: Effect of inlet angle of Line 3, β_1, on pump performance

4.2.4. Effect of outlet angle of Line 3

β_2 values from 10° to 22° were selected to investigate its effect on single-channel pump performance. The impeller design parameters with an outlet angle of Line 3 are listed in **Table 7**.

Table 7: Impeller design parameters with different outlet angles of line 3, $\boldsymbol{\beta_2}$

Inlet diameter coefficient (K_{D_1})	4	4	4	4
Outlet diameter coefficient (K_{D_2})	10.3	10.3	10.3	10.3
Angle (β_1)	9	9	9	9
Angle (β_2)	**10**	**14**	**18**	**22**
Angle (β_0)	37	37	37	37

The performance curves for the various β_2 values are shown in **Figure 10**. As β_2 increased, the pump head increased slightly, and the BEP was achieved at a higher flow rate. β_2 = 18° resulted in a high head, and its BEP was consistent with the design point. At β_2 = 22°, the BEP deviated from the design point. Similar to the investigation of the inlet angle of Line 3, the effects of various

outlet angles of Line 3 on the pump performance curves were insignificant.

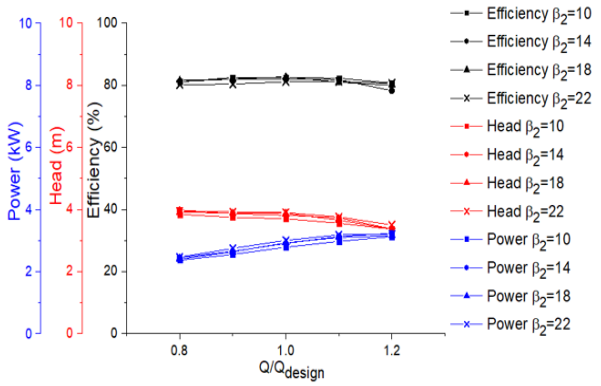

Figure 10: Effect of outlet angle of Line 3 β_2 on pump performance

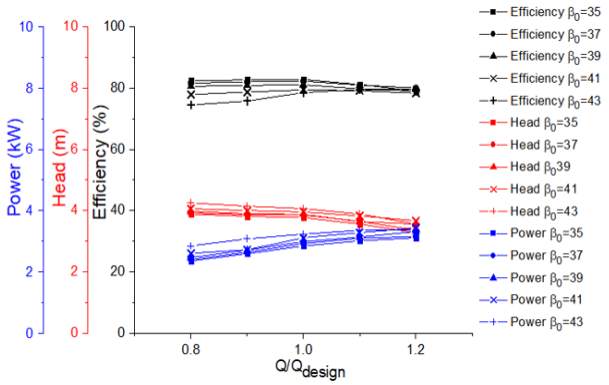

Figure 11: Effect of outlet angle of line 1 β_0 on pump performance

Table 8: Impeller design parameters with different outlet angles of line 1, $\boldsymbol{\beta_0}$

Inlet diameter coefficient (K_{D_1})	4	4	4	4	4
Outlet diameter coefficient (K_{D_2})	10.3	10.3	10.3	10.3	10.3
Angle (β_1)	9	9	9	9	9
Angle (β_2)	18	18	18	18	18
Angle ($\boldsymbol{\beta_0}$)	**35**	**37**	**39**	**41**	**43**

4.2.4. Effect of outlet angle of Line 1

Table 8 presents the impeller design parameters for different outlet angles of line 1 β_0. Five cases of β_0 ranging from 35° to 43° were selected to investigate the effect of the outlet angle of the inlet on the single-channel pump performance. The performance curves for the various β_0 values are shown in **Figure 11**. When the pump efficiency decreased, the pump head elevated, and the BEP shifted from partial to full load conditions. Subsequently, the impeller outlet angle of the inlet, β_0, was changed from a smaller to a larger value. For β_0= 41°, the head satisfied the design specifications, and its BEP was consistent with the design point. Meanwhile, for β_0= 43°, the BEP was 1.1Q_{design}.

4.3. Effects of impeller out cross-sectional shapes on pump performance and internal flow characteristics

New values for the parameter of the base model were selected after investigating the effects of the design parameters on the single-channel pump performance. A comparison between the initial and final values of the design parameters is presented in **Table 9**. Using the final impeller design parameters, different cross-section impellers were implemented, including circular, combined circular and rectangular, and rectangular cross-sections, as shown in **Figure 12**. **Figure 13** presents the single-channel pump performance curves for different cross-sectional impellers. The efficiency and head of the circular cross-sectional impeller model were slightly better than those of the other cross-sectional impeller models.

Table 9: Design parameters of single-channel pump impeller base model

Item	Nomenclature [Unit]	Initial Value	Final value
Impeller outlet diameter	D_2 [mm]	330	330
Outlet diameter coefficient	K_{D_2}	10.3	10.3
Impeller inlet diameter	D_1 [mm]	185	185
Inlet diameter coefficient	K_{D_1}	4	4
Outlet angle of line 1	β_0 [°]	37	41
Total wrap angle of line 1	φ_1 [°]	150	132
Inlet angle of line 3	β_1 [°]	8	9
Outlet angle of line 3	β_2 [°]	10	18
Total wrap angle of line 3	φ_2 [°]	297	195

The losses of the impeller and volute are expressed as shown in **Equations (6)** and **(7)**, respectively:

$$h_{loss-impeller} = \frac{\frac{T\omega}{Q} - \Delta p_t}{\rho g H} \times 100\% \quad (6)$$

$$h_{loss-volute} = \frac{\Delta p_t}{\rho g H} \times 100\%, \quad (7)$$

where $h_{loss-impeller}$ is the total loss of the pump impeller,

$h_{loss-volute}$ the total loss for the pump volute, and Δp_t the total pressure difference in the respective components of the pump.

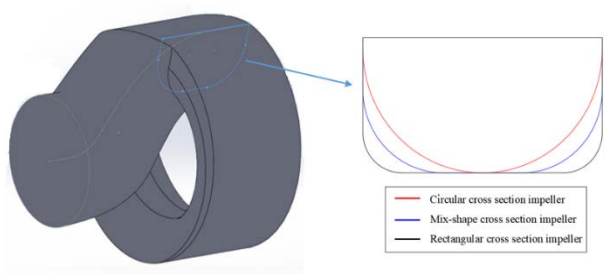

Figure 12: Three types of impeller outlet cross-sectional shapes

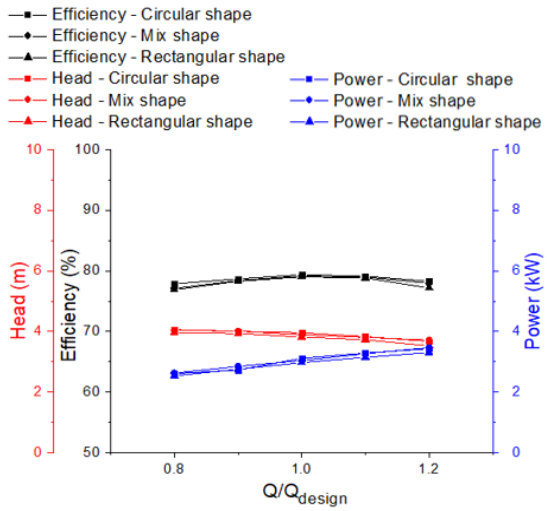

Figure 13: Pump performance curves of single-channel pump models with different impeller outlet cross-sectional shapes

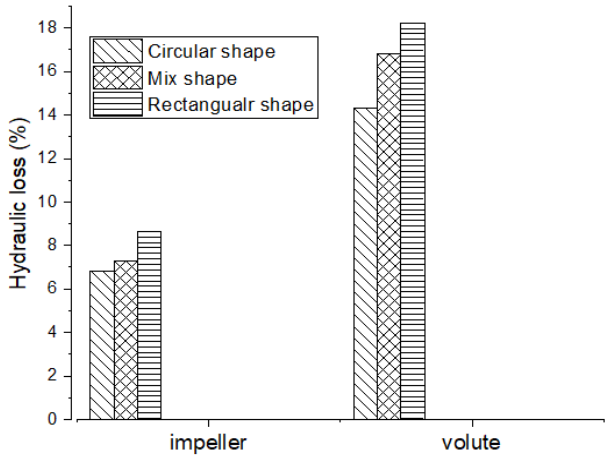

Figure 14: Loss analysis of impeller and volute among different impeller outlet cross-sectional shapes

The loss analysis of the impeller and volute for the different cross-sectional impellers under the design condition is presented in **Figure 14**. In both the impeller and volute domains, the hydraulic loss in the circular cross-sectional impeller was lower than that in the combined and rectangular cross-sectional impellers. Therefore, the pump efficiency of the impeller-out circular cross-section model was better than that of the combined shape and rectangular cross-section models.

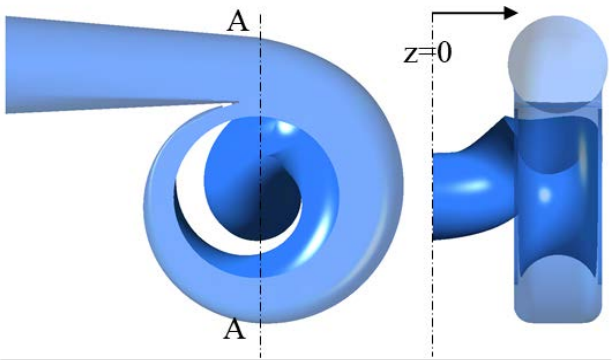

Figure 15: Measurement location in single-channel pump

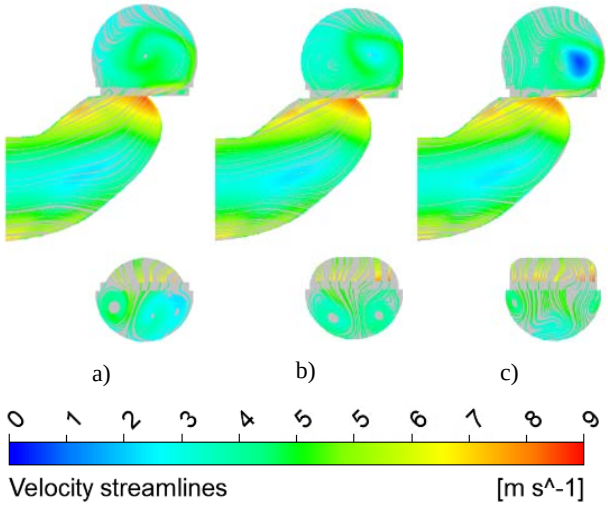

Figure 16: Velocity streamlines distribution in single-channel pump models with a) circular, b) combined, and c) rectangular outlet impellers at plane A–A

Figure 15 shows the measurement locations of the single-channel pump. The velocity streamline distributions of the various cross-section impellers and volutes are shown in **Figure 16**. The flow characteristics inside the impeller were not affected significantly by the change in the cross-section. However, a low-velocity swirl flow was observed at the volute of the rectangular cross-sectional impeller. The occurrence of the swirl flow can cause a slightly worse pump performance in the impeller-out rectangular cross-section model.

4.4. Cavitation analysis

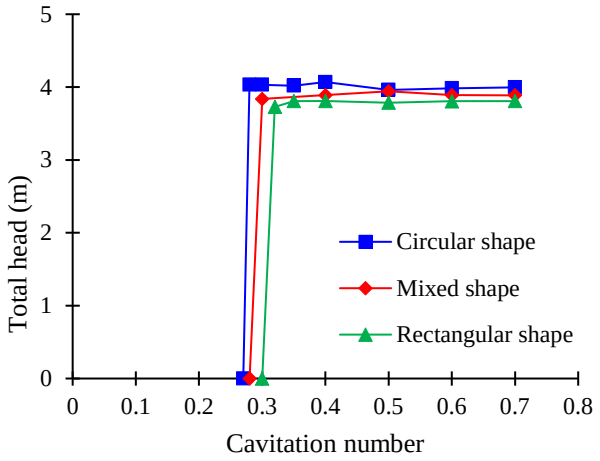

Figure 17: Suction performance of single-channel pump models with different impeller outlet cross-sectional shapes

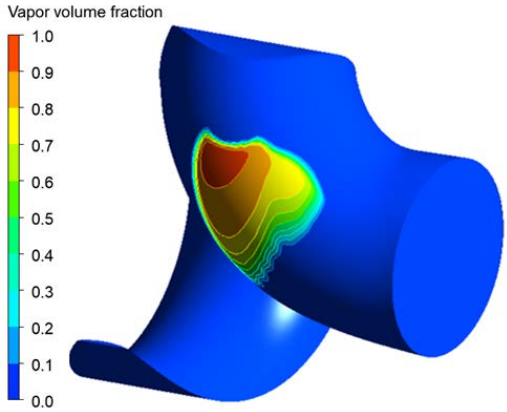

Figure 18: Cavitation inception of single-channel pump

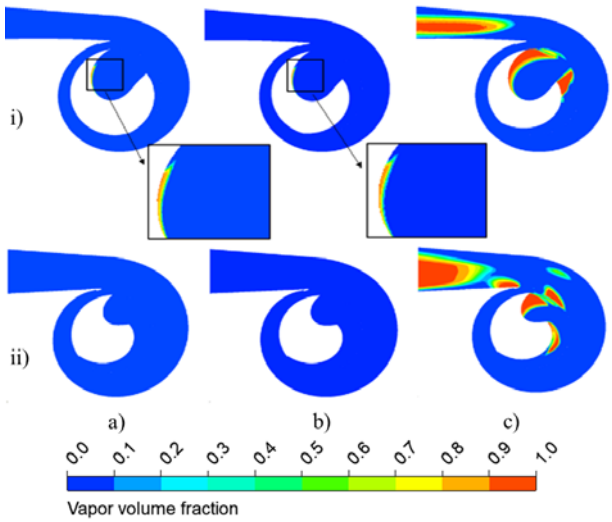

Figure 19: Vapor volume fraction distribution in single-channel pump models with a) circular, b) combined, and c) rectangular cross-sections at σ = 0.3 i) z =175 mm, and ii) z = 250 mm

Figure 17 shows the suction performance comparison of the single-channel pump models with various cross-sectional impellers via CFD analysis. The cavitation number (σ) is expressed as shown in **Equation (8)**.

$$\sigma = \frac{NPSH}{H} = \frac{p_0 - p_v}{\rho g H}, \tag{8}$$

where p_0 is the pump inlet pressure, p_v the saturated vapor pressure, ρ the water density, g the gravity, $NPSH$ the net positive suction head, and H the total head.

Figure 17 shows the suction performance of the single-channel pump. The critical cavitation numbers for the circular, combined, and rectangular cross-sectional impellers were 0.28, 0.30, and 0.32, respectively. The cavitation inception location in the single-channel pump is shown in **Figure 18,** where 0 indicates water and 1 indicates vapor cavity inception. The result of the vapor volume of the fraction distribution at the cavitation coefficient number σ = 0.3 is presented in **Figure 19**. As shown, the vapor volume of the fraction was prominent in the rectangular cross-section impeller and volute, which implies that it is susceptible to cavitation. Moreover, at σ =0.3, the circular and combined cross-sectional impellers suppressed cavitation significantly.

5. Conclusions

In this study, an impeller design methodology for a single-channel pump model was proposed. Impeller design parameters contribute significantly to the impeller flow passage, which directly affects the performance of the single-channel pump. In addition, various impeller outlet cross-sectional shapes, including circular, combined, and rectangular shapes, were investigated based on hydraulic and suction performances as well as internal flow characteristics to identify a suitable model for the transfer of sensitive goods.

The parametric study of a single-channel pump indicated that the outlet angle, impeller inlet, and impeller outlet diameter significantly affected pump performance. The xxx of head and efficiency of single channel pump decreased as the inlet diameter increased. When the impeller outlet diameter decreased, the BEP was achieved under partial load conditions. The BEP shifted from partial to full load conditions as the outlet angle of Line 1 increased. The inlet and outlet angles of Line 3 did not significantly affect the pump head and efficiency. The parametric study showed that K_{D_1} = 4, K_{D_1} = 10.3, β_1 = 9, β_2 = 18, and β_0 = 41 were

the optimal values for the conceptual design of the single-channel pump. The final design parameters increased the total head length of the single-channel pump from 3.66 to 3.96 m at the design flow rate. Therefore, the final conceptual design of the single-channel pump was consistent with the design specifications.

Circular, combined, and rectangular cross-sections were designed to improve the pump performance. The impeller with a circular outlet cross-sectional shape showed better pump efficiency and suction performance than the impellers with combined and rectangular outlet cross-sections. The pump efficiencies of the impellers with rectangular, combined, and circular cross-sections were 79.1%, 79.3%, and 79.5%, respectively. The velocity streamlines indicated that the secondary flow in the rectangular-outlet impeller was more intense than that in the circular-outlet impeller. The critical cavitation number decreased from 0.32 to 0.28 when the circular cross-section impeller was used. Therefore, a circular cross-sectional impeller is preferable for achieving a uniform flow distribution, high efficiency, and good suction performance in a single-channel pump.

Author Contributions

Conceptualization, T. H. M. Hoang, U. Shrestha and Y. D. Choi; Methodology, T. H. M. Hoang; Software, T. H. M. Hoang and U. Shrestha; Validation, T. H. M. Hoang, U. Shrestha and Y. D. Choi; Formal Analysis, T. H. M. Hoang; Investigation, T. H. M. Hoang; Resources, T. H. M. Hoang and U. Shrestha; Data Curation, T. H. M. Hoang and U. Shrestha; Writing—Original T. H. M. Hoang; Writing—Review & Editing, Y. D. Choi; Supervision, Y. D. Choi; Funding Acquisition, Y. D. Choi.

References

[1] X. F. Guan, Modern Pump Theory and Design, Beijing, China, Astronaut Publishing House, 2011 (in Chinese).

[2] J. H. Kim, B. M. Cho, Y. S. Kim, Y. S. Choi, K. Y. Kim, J. H. Kim, Y. Cho, “Optimization of a single-channel pump impeller for wastewater treatment,” International Journal of Fluid Machinery and Systems, vol. 9, no. 4, pp. 370-381, 2016.

[3] M. Guo and Y. D. Choi, “Effect of impeller blade thickness in the performance and internal flow characteristics of a single channel pump model,” The KSFM Journal of Fluid Machinery, vol. 23, no. 1, pp. 15-22, 2020.

[4] X. Wu, H. Liu, and J. Ding, “Performance prediction of single-channel centrifugal pump with steady and unsteady calculation and working condition adaptability for turbulence model,” Transactions of the Chinese Society of Agricultural Engineering, vol. 220, Part E, pp. 85-91, 2006.

[5] J. Keays and C. Meskell, “A study of the behaviour of a single-bladed waste-water pump,” Journal of Process Mechanical Engineering, vol. 220, no. 2, pp. 79-87, 2006.

[6] J. Pei, S. Yuan, and J. Yuan, “Fluid-structure coupling effects on periodically transient flow of a single-blade sewage centrifugal pump,” Journal of Mechanical Science and Technology, vol. 27, pp. 2015-2023, 2013.

[7] O. Litfin, A. Delgado, K. Haddad, and H. Klein, “Numerical and experimental investigation of trailing edge modifications of centrifugal wastewater pump impellers,” Proceedings of the ASME 2017 Fluids Engineering Division Summer Meeting, 2017.

[8] A. J. Stepanoff, Centrifugal and Axial Flow Pumps: Theory, Design, and Application, 2nd edition, John Wiley & Sons, Inc, 1957.

[9] ANSYS Inc., ANSYS CFX Documentation, Ver. 18.1, http://www.ansys.com, Accessed, 2019.

[10] ANSYS ICEM., ANSYS ICEM Documentation, Ver. 18.1, http://www.ansys.com, Accessed, 2018.

[11] F. R. Menter, M. Kuntz, and R. Langtry, “Ten years of industrial experience with the SST turbulence model,” Proceedings of the 4th International Symposium on Turbulence, Heat and Mass Transfer, vol. 4, no. 1, pp. 625-632, 2003.